

# Mechanical and corrosion properties of biodegradable Mg-1.5Mn-1Ca-xSr alloys

X Sun<sup>1,\*</sup>, S Y Sun<sup>2</sup>, Y H Ning<sup>1</sup> and Y T Ning<sup>3</sup>

<sup>1</sup> Datang northeast electric power test and research institute, Changchun, Jilin, China, No. 3195 Weishan Street, Changchun, 130000, China.

<sup>2</sup> Brand School of Engineering and Technology, Changchun Vocational Institute Of Technology, Changchun 130033, China

<sup>3</sup> State Grid Jilin Electric Power Company, Changchun, Jilin, China, No. 4969 Renmin Street, Changchun, 130000, China.

E-mail: 380541075@qq.com

**Abstract.** The mechanical properties and corrosion mechanism of both as-cast and solution-naturally age (T4) treated Mg-1.5Mn-1Ca-xSr alloys were investigated. The results showed that Sr is helpful to decrease grain size and increase the strength. The corrosion process of alloys was mainly determined by the quantity and distribution of second phases. Mg<sub>17</sub>Sr<sub>2</sub>,  $\alpha$ -Mn and Ca-Sr phases acted as cathodes accelerated the corrosion of Mg<sub>2</sub>Ca anodic phase and  $\alpha$ -Mg matrix. However, continuous distributed Mg<sub>17</sub>Sr<sub>2</sub> was beneficial to resist the happening of localized corrosion because of its barrier effect. T4 treatment could significantly improve the mechanical properties and corrosion resistance of Mg alloys because of the dissolution of Mg<sub>2</sub>Ca phase and the dispersive distribution of Mg<sub>17</sub>Sr<sub>2</sub> and  $\alpha$ -Mn phases.

**Keywords:** Biodegradable; T4 treatment; Microstructure; Mechanical properties; Corrosion.

## 1. Introduction

The Mg and its alloys have attracted considerable attention in recent years as potential biodegradable implant materials due to their good biocompatibility [1-3]. The most obvious advantage of magnesium compared with the other biomedical metal material is the relatively negative standard electrode potential (-2.37 V at 25 °C) and its biological safety, which make magnesium able to be biodegraded in human body environment [4,5]. Hence, the second removal surgical operation for implants could be avoided. The suitable elastic modulus of magnesium (40~45GPa) is similar to natural bone, which will effectively prevent the happening of “stress-shield” phenomenon [6]. However, there are also some concerns in using Mg and Mg alloys for load-bearing implant materials. One is the relative poor mechanical performance compared with the other commonly used metallic implants. The second is the uncertain capability of Mg alloys due to its low corrosion resistance [4,7]. Thirdly, the biocompatibility of current Mg alloys is still inadequate for biomedical applications.

T4 treatment and alloying are two promising ways to overcome the disadvantages mentioned above [8]. As a common means to refine the microstructure of castings, T4 treatment can help to dissolve and disperse second phases, which is helpful to eliminate the negative effect of coarse phases on the mechanical and corrosion properties. The addition of alloying elements into Mg alloys would increase



the electrode potential of Mg matrix and support solution strengthening and second phase strengthening effects. Base on the toxicological date issued by World Health Organization (WHO) [9, 10], Ca, Zn, Mn (essential trace elements for human body) and Si, Sr, Al, RE (probably essential for human body) can be chosen as potential healthy alloying elements for the application of biological metal. Mg alloys with Al or RE had been proved to have good mechanical properties and corrosion resistance. However, due to the uncertain biological safety of Al and RE, there is always a lot of dispute revolved about their addition into Mg alloys [11]. Mg-Ca system alloys are the most promising biomedical magnesium alloys due to the good biocompatibility of Ca [12,13], however, the mechanical properties and corrosion resistance of Mg-Ca system alloys are not good enough. Mg-Zn system alloys with the addition of Ca or/and Mn as alloying elements had also been investigated [14-17]. It is believed that the corrosion rate of Mg alloys increased with increasing content of Zn and the second phases have great influence on corrosion resistance [15-18], which indicating that a newly developed alloy without controversial alloying elements and has less amount of second phase may be a promising degradable biomedical material with a suitable mechanical and corrosion properties.

Ca is one of the most promising biocompatible alloying elements for Mg alloys. It is regarded as the most abundant mineral in the body and plays a crucial role in the formation of bone. The addition of Ca can not only improve the metallurgical quality of magnesium alloys, but also reduce oxidation during smelting and heat treatment processing [19]. Mn has little effect on the tensile strength of Mg alloys. However, Mn can significantly improve the corrosion resistance of Mg alloys by removing iron and other heavy-metal elements. Mn has no toxic and plays a primary role in the activation of multiple enzyme system, i.e., hydrolases, kinases, transferases, decarboxylases and mitochondrial respiration [20,21]. Sr is always known as a grain refiner for magnesium and is beneficial to improve the mechanical properties and corrosion resistance for certain Mg alloys [22,23]. Moreover, Sr can also improve bone strength and bone mineral density, and is used in the treatment for osteoporosis. Sr has been shown to decrease the osteoclast activity and increase the replication of pre-osteoblast cells, thereby decreasing the bone resorption while stimulating bone formation [24-26]. In consideration of human safety, Mn, Ca and Sr were finally chosen as alloying elements in this work to improve both the corrosion resistance and mechanical properties of Mg. The probability of Mg-Mn-Ca and Mg-Mn-Ca-Sr alloys used as biodegradable implant materials with low corrosion rate and high mechanical property was invested.

## 2. Materials and methods

### 2.1. Preparation of magnesium alloys

Two alloys with targeted compositions of Mg-1.5Mn-1Ca and Mg-1.5Mn-1Ca-1Sr alloys (wt. %, hereafter) were prepared in a self-assembly non-ferrous alloy melting equipment. The alloying components were melted around 1053 K (780 °C). After proper treatment, magnesium melt poured into a copper mold at 1023 K (750 °C) and cooled to room temperature under the protection of high purity argon atmosphere (99.999 %). During the melting process, the melt was mechanical stirred. Cast bars that cut from the ingot were then solution-treated at 480 °C for 16 h, and quenched rapidly in water. The analyzed chemical compositions of prepared alloys were determined by inductively coupled plasma-atomic emission spectrometer (ICP-AES), the results are given in table 1.

**Table 1.** Chemical compositions of Mg-1.5Mn-1Ca-xSr alloys (wt. %).

Alloys	Mn	Ca	Sr	Mg
Mg-1.5Mn-1Ca	1.585	1.049	-	Bal
Mg-1.5Mn-1Ca-1Sr	1.614	1.048	0.9867	Bal

### 2.2. Microstructure and Mechanical test

Samples for microstructure observation were cut from the ingot and the solution-treated bar. For metallographic observation, the specimens were mechanically polished and etched with a dilute solution of 4% nitric acid in methanol. Microstructural analyses were examined by using Optical microscopy and scanning electronic microscope (SEM) equipped with an energy dispersive spectrometer (EDS). Phase identification was performed on the bulk samples by using EDS and X-ray diffraction (XRD). Mechanical testing samples were prepared according to ASTM B557-06. Tensile tests were processed by MTS810 universal testing machine with a strain rate of  $1 \times 10^{-3} \text{ s}^{-1}$  at room temperature. At least 3 samples were tested for each condition.

### 2.3. Preparation of corrosion media

In order to evaluate the degradation properties, electrochemical measurements and immersion tests were performed in simulated body fluid (SBF), containing NaCl 8.035 g/l, KCl 0.225 g/l, CaCl<sub>2</sub> 0.292 g/l, NaHCO<sub>3</sub> 0.355 g/l, MgCl<sub>2</sub>·6H<sub>2</sub>O 0.311 g/l, Na<sub>2</sub>SO<sub>4</sub> 0.072 g/l, KH<sub>2</sub>PO<sub>4</sub>·3H<sub>2</sub>O 0.231 g/l [16]. The pH value of SBF was adjusted to a neutral level (pH =  $7 \pm 0.1$ ). The solution temperature was controlled around  $37 \pm 0.5 \text{ }^{\circ}\text{C}$ , which is aim to simulate human body environment. Rectangular specimens for corrosion tests were molded into epoxy resin with only one side of  $1 \text{ cm}^2$  exposed for the test

### 2.4. Electrochemical test

The potentiodynamic polarisation test was carried out at  $37 \pm 1 \text{ }^{\circ}\text{C}$  in a beaker containing 300 ml of SBF solution by using a standard three-electrode configuration: the saturated calomel as a reference, a graphite electrode as the counter and the sample as the working electrode. The samples were encapsulated into epoxy resin with a working surface of  $1 \text{ cm}^2$ . Prior to the experiment, the rectangular samples were ground up to 2000 grit by SiC paper, followed by washing with distilled water and acetone. The polarization curve was measured at a scan rate of 0.5 mV/s.

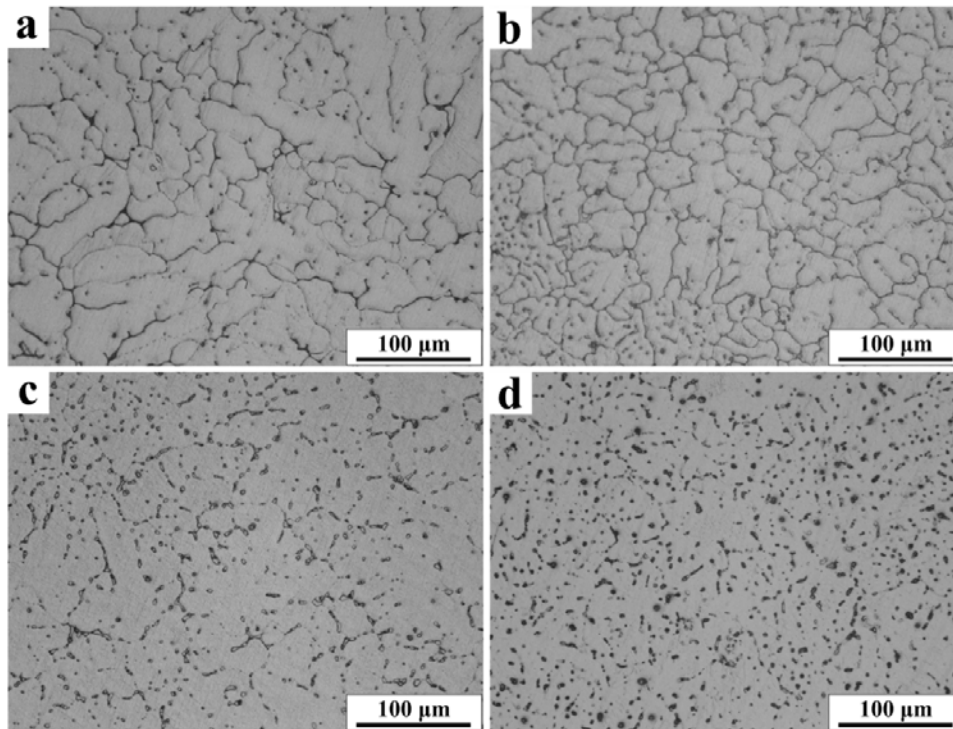
### 2.5. Immersion test

After grinded with SiC paper up to 2000 grit, the rectangular samples were rinsed with distilled water and dried. Every sample was placed in a beaker containing 250 mL of SBF solution. Hydrogen bubbles resulting from corrosion of each specimen were collected in a burette, so the volume of the generated hydrogen could be measured through reading the solution level in the burette. Detailed procedures for the hydrogen measurement have been reported elsewhere [27]. After short-term and long-term immersion test, samples were taken out of the soaking medium and cleaned in boiling 15% CrO<sub>3</sub> + 1% AgCrO<sub>4</sub> solution for 10 min to remove the corrosion products. Then the surface morphology without corrosion products could be observed by using laser scanning confocal microscope (LSCM) and SEM.

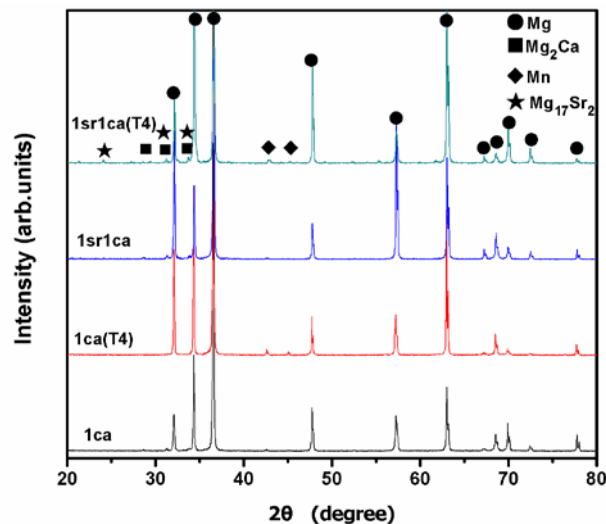
## 3. Results and discussion

### 3.1. Microstructure and phase constitution of Mg-1.5Mn-1Ca-xSr alloys

The microstructures of as-cast and T4 treated Mg-1.5Mn-1Ca-xSr alloys are shown in figure 1. As can be seen in figure 1, Mg-1.5Mn-1Ca-xSr alloys are mainly consisted of dendrites. Grain size decreases with the addition of Sr. The second phases are mainly arranged along the grain boundaries, some lies within the grains. T4 treatment partly dissolved the second phases and refined grain boundaries (figure 1 c and d). Figure 2 shows the XRD patterns of as-cast and T4 treated Mg-1.5Mn-1Ca-xSr alloys, which showed the existence of Mg<sub>2</sub>Ca phase, Mg<sub>17</sub>Sr<sub>2</sub> phase and  $\alpha$ -Mn phase.

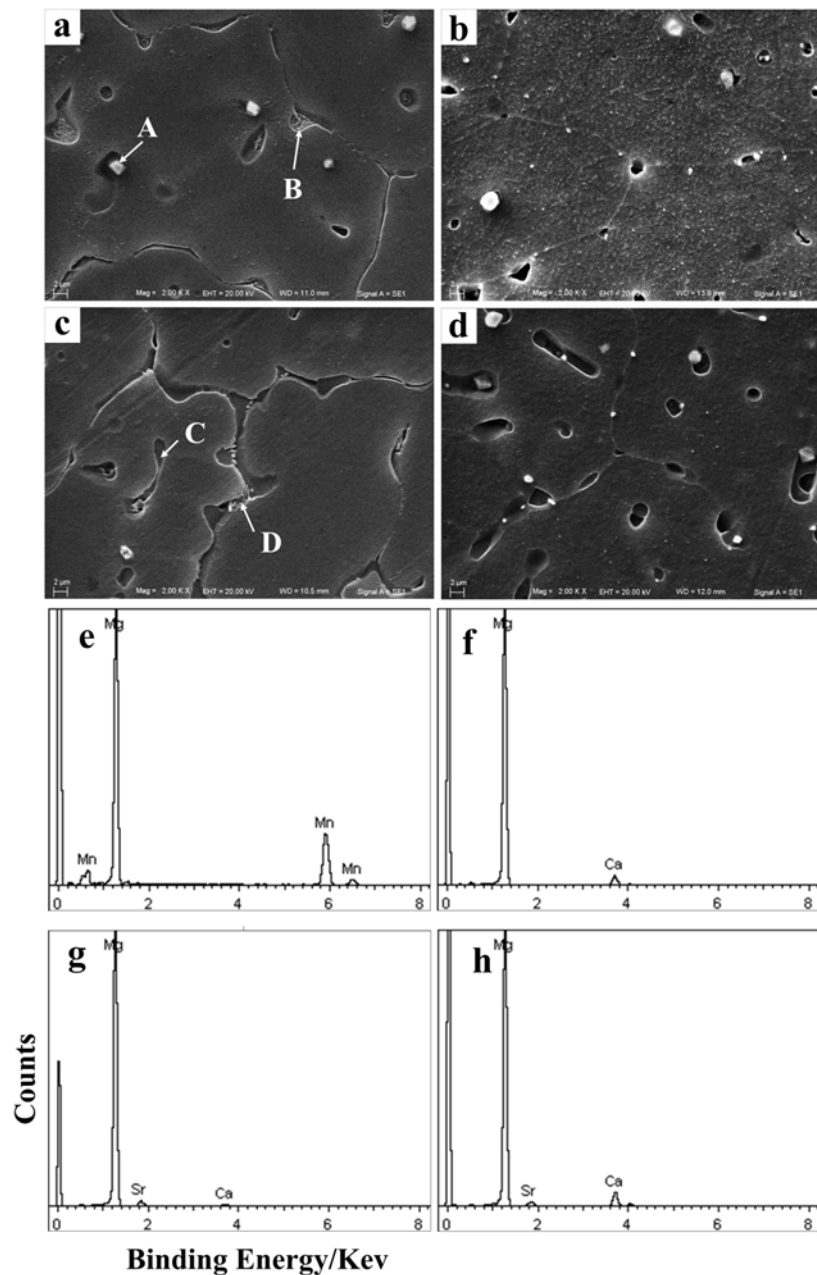


**Figure 1.** Optical micrograph of (a) as-cast Mg-1.5Mn-1Ca alloy, (b) as-cast Mg-1.5Mn-1Ca-1Sr alloy, (c) T4 treated Mg-1.5Mn-1Ca alloy, (d) T4 treated Mg-1.5Mn-1Ca-1Sr alloy.



**Figure 2.** XRD analysis of as-cast and T4 treated Mg-1.5Mn-1Ca-xSr alloys.

As for the reason that the grain refinement in figure 1, it was widely accepted that alloying elements process a strong segregation ability in melt alloy and form intensive constitutional undercooling in a diffusion layer ahead of the advancing solid/liquid interface which restricts the grain growth and promotes the nucleation of the primary Mg, thus refines the grain size [28]. The refinement efficiency of an element can be determined by the calculation of a growth restriction factor (GRF) which can be calculated by using binary phase diagrams. In GRF formula:  $\sum m_i c_{o,i} (k_i - 1)$ , where  $m_i$  is the slope of the liquidus line (assumed to be a straight line),  $k_i$  is the distribution coefficient, and  $C_{o,i}$  is the initial concentration of element  $i$ . According to Mg/Sr binary phase diagram, Sr shows a high GRF, which indicated that Sr could effectively refine grains.



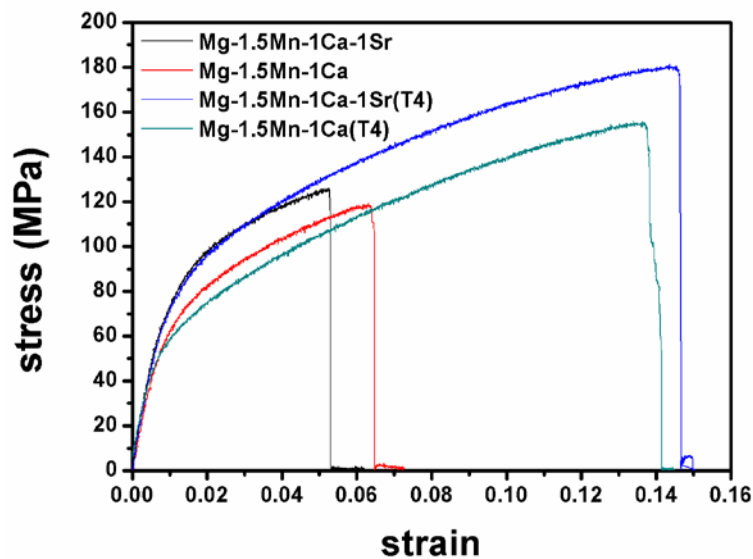
**Figure 3.** SEM microstructure of (a) as-cast Mg-1.5Mn-1Ca alloy, (b) T4 treated Mg-1.5Mn-1Ca alloy, (c) as-cast Mg-1.5Mn-1Ca-1Sr alloy, (d) T4 treated Mg-1.5Mn-1Ca-1Sr alloy, (e - f) EDS result of the sites from A to D in Fig. 3 (a) and (c).

Figure 3 (a-d) show the distribution and morphology of  $\alpha$ -Mg +  $\alpha$ -Mn peritectic structure (Site A),  $\alpha$ -Mg +  $\text{Mg}_2\text{Ca}$  lamellar eutectic (Site B) and  $\alpha$ -Mg +  $\text{Mg}_2\text{Ca}$  +  $\text{Mg}_{17}\text{Sr}_2$  divorced eutectic structure, which may also be the Ca/Sr-rich phases [29], (Sites C and D). Figure 3 (e-h) shows the EDS results of sites from A to D. From the morphology of different eutectic structures, it could be distinguished that the phase which contains more  $\text{Mg}_{17}\text{Sr}_2$  is more compact. Compared with as-cast alloy, T4 treated alloy has finer grain boundaries. By T4 treatment,  $\text{Mg}_2\text{Ca}$  partly dissolved in  $\alpha$ -Mg matrix and  $\alpha$ -Mn phase had the phenomenon of dissolution-re-precipitation which was caused by the effect of naturally age. The supersaturated  $\alpha$ -Mn precipitated dispersedly from  $\alpha$ -Mg in rod-like shape, which is consistent

with the results observed in earlier study [22] and contributes to the microstructure homogenization. T4 treatment had little effect on the dissolution of  $\text{Mg}_{17}\text{Sr}_2$  because of the low solubility of Sr in Mg.

### 3.2. Mechanical properties of Mg-1.5Mn-1Ca-xSr alloys

Figure 4 shows the stress-strain curves of as-cast and T4 treated Mg-1.5Mn-1Ca-xSr alloys. The detail data of tensile test are listed in table 2. The addition of Sr is helpful to improve the yield strength (YS) and ultimate tensile strength (UTS), but decreases the elongation. After T4 treatment, both the UTS and the elongation of Mg-1.5Mn-1Ca-xSr alloys increase significantly, except the YS decrease slightly. The mechanical properties of Mg-1.5Mn-1Ca-xSr alloys are mainly determined by their microstructure. In Figure 1 the grain size decreased with the addition of Sr, which contributes to the increase of yield strength according to Hall-Petch law [30]. The second phases that distributed along the boundaries and in grains provided second phase strengthening effect which increased the strength but decreased the elongation of alloys. However, too much volume fraction of second phase is also harmful. It had been reported that the lamellar  $\text{Mg}_2\text{Ca}$  phase decreased the ductility of Mg-0.9Ca alloy. It was thought that  $\text{Mg}_2\text{Ca}$  phase dispersed at the grain boundary could be the crack source for Mg-Ca alloy [31]. By treatment,  $\text{Mg}_2\text{Ca}$  phase dissolved into matrix and the distribution of  $\text{Mg}_{17}\text{Sr}_2$  phase and  $\alpha\text{-Mn}$  phase are more diffuse, which provided solution strengthening effect and reduced the cracking tendency. The combined effect of solution strengthening and second phase strengthening contributes to the significant increase of the tensile properties of T4 treated Mg-1.5Mn-1Ca-xSr alloys.



**Figure 4.** Typical stress-strain curves of as-cast and T4 treated Mg-1.5Mn-1Ca-xSr alloys.

**Table 2.** Mechanical properties of as-cast and T4 treated Mg-1.5Mn-1Ca-xSr alloys.

Alloy	YS (MPa)	UTS (MPa)	Elongation (%)
Mg-1.5Mn-1Ca	58±4	119±6	6.3±0.62
Mg-1.5Mn-1Ca(T4)	55±3	155±5	13.6±0.70
Mg-1.5Mn-1Ca-1Sr	78±2	125±4	5.3±0.42
Mg-1.5Mn-1Ca-1Sr(T4)	76±2	180±3	14.5±0.66

### 3.3. Electrochemical properties of Mg-1.5Mn-1Ca-xSr alloys

The electrochemical polarization curves of as-cast and T4 treated Mg-1.5Mn-1Ca-xSr alloys in SBF solution are shown in figure 5. Generally, the cathodic polarization curves are assumed to represent the cathodic hydrogen evolution through water reduction, while the anodic polarization curves represent the dissolution of magnesium. In figure. 5, no current plateau is observed in the anodic region of Mg-

1.5Mn-1Ca-xSr alloys. The addition of Sr moves the corrosion potential ( $E_{corr}$ ) to a more negative direction. By T4 treatment, the corrosion potential of both alloys increased slightly and followed by the decrease of corrosion current density, which indicated the enhancement of corrosion resistance. The detail electrochemical parameters of the electrochemical polarization curves in figure. 5 are listed in table 3. The  $E_{corr}$  and  $I_{corr}$  were derived from the plots by Tafel extrapolation. The corrosion rate ( $P_i$ ) can be calculated using the conversion equation according to ASTM-G102-89:  $P_i = 22.85 \times I_{corr}$ , where the  $P_i$  is given in mm/yr and  $I_{corr}$  in mA/cm<sup>2</sup>.

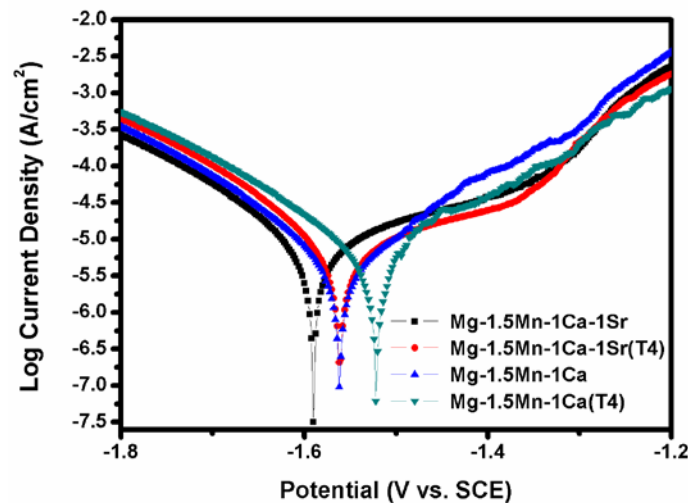


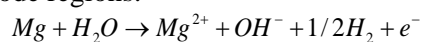
**Figure 5.** Tafel curves of as-cast and T4 treated Mg-1.5Mn-1Ca-xSr alloys immersed in SBF.

**Table 3.** Electrochemical parameters of as-cast and T4 treated Mg-1.5Mn-1Ca-xSr alloys in SBF solution.

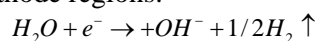
Alloys	$E_{corr}$ (mV)	$i_{corr}$ ( $\mu\text{A}/\text{cm}^2$ )	$P_i$ (mm/yr)
Mg-1.5Mn-1Ca	-1562	9.29	0.21
Mg-1.5Mn-1Ca(T4)	-1524	7.36	0.17
Mg-1.5Mn-1Ca-1Sr	-1596	17.8	0.4
Mg-1.5Mn-1Ca-1Sr (T4)	-1565	6.61	0.15

### 3.4. Immersion tests

Because of the “negative difference effect”, hydrogen evolution is more effective than means of Tafel extrapolation on polarization curves to measure the corrosion rate of magnesium alloys [32]. Figure 6 presents the hydrogen evolution results of immersion test in SBF, which shows that the average hydrogen evolution rates of T4 treated Mg-1.5Mn-1Ca-xSr alloys are much less than that of as-cast alloys. The addition of Sr decreases the corrosion rate slightly. All specimens exhibit a decrease in hydrogen evolution rate with increasing immersion time. It is shown that all specimens had a relative high hydrogen evolution rate and undergone a quickly corrosion period in the first 7h, and then hydrogen evolution rate gradually go to a relative steady value, which indicated that the corrosion process enter the stable period. This result could be explained by the electrochemical corrosion mechanisms of magnesium in neutral corrosive mediums proposed according to G. Song [27]. At the anode regions:

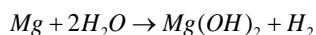


The phenomenon of anodic hydrogen evolution was only special for magnesium alloys. At the cathode regions:





The total reaction:



So, in the beginning of corrosion process, the anode quickly dissolved and  $\text{H}_2$  released at the cathode. The corrosion products, which are mainly composed of  $\text{Mg}(\text{OH})_2$ , is loose and could support little protective effect. So in this period,  $\text{Mg}^{2+}$  could still diffuse toward the exterior surface of corrosion product layer and electrolytes diffuse toward the interior surface of corrosion product layer.  $\text{Mg}^{2+}$  and electrolytes meet inside the film layer and continue to form corrosion products. With the increase of immersion time, the corrosion product layer becomes more and more compact which restrict the diffusion of ions inside the layer. When the dissolution and formation of corrosion product layer keeps dynamic balance, the corrosion process advanced into the stable period in which the corrosion product layer stop growing and could support a certain protective effect. So the corrosion rates of the specimens decrease noticeably and keep on a relative low standard after the initial 7h.

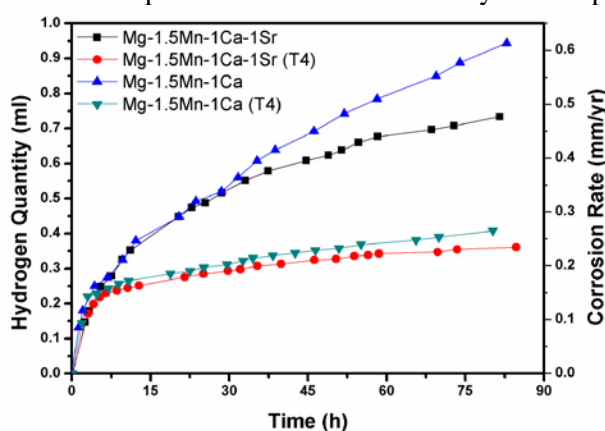


**Figure 6.** Hydrogen evolution for as-cast and T4 treated Mg-1.5Mn-1Ca-xSr alloys immersed in SBF.

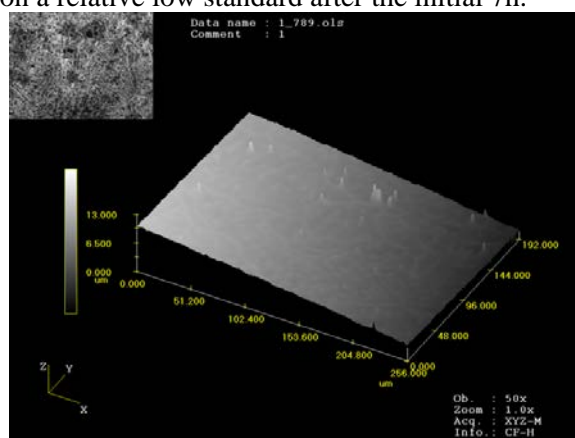


**Figure 7.** Laser scanning confocal microscope (LSCM) image of as-cast Mg-1.5Mn-1Ca-1Sr alloys immersed in SBF for 3 min.

### 3.5. Corrosion morphology analysis

In order to investigate the corrosion process and corrosion mechanism of Mg-1.5Mn-1Ca-xSr alloys in detail, the corroded surfaces of short-term (3 min) and long-term (52 h) exposure samples were analyzed under LSCM and SEM. Selected LSCM and SEM micrographs are shown in figure 7 and figure 8. Figure 7 shows the short-term corrosion morphology of as-cast Mg-1.5Mn-1Ca-1Sr alloy, from which it could be seen that the  $\alpha$ -Mg matrix act as anodic was priority corroded. The raised parts are the second phases and the distinct peaks are  $\alpha$ -Mn phase. Figure 8 shows the long-term corrosion morphology of as-cast and T4 treated Mg-1.5Mn-1Ca-xSr alloys after removed the corrosion products. From figure 8, it could be observed that the corrosion sites mainly located around the second phases, especially  $\text{Mg}_2\text{Ca}$  act as anodic phase was first corroded. Pitting occurs both in boundaries and grains. After T4 treatment, the corrosion degree of Mg-1.5Mn-1Ca-xSr alloys is weakened and the corrosion morphologies become smooth (figure 8c, d, f and g). But the residual  $\text{Mg}_2\text{Ca}$  and dispersedly distributed  $\alpha$ -Mn phases still have a serious effect on the corrosion process. In figure 8, it could be observed that the T4 treated Mg-1.5Mn-1Ca-1Sr alloy has the most evenly morphology and there is no apparent corrosion around  $\text{Mg}_{17}\text{Sr}_2$  and  $\alpha$ -Mn phase.

The corrosion mechanism of Mg-1.5Mn-1Ca-xSr alloys is significantly controlled by the changes in quantity, distribution, configuration and size of the second phases. The effective cathodes phases  $\text{Mg}_{17}\text{Sr}_2$  and  $\alpha$ -Mn would cause micro-galvanic corrosion with anode phase  $\text{Mg}_2\text{Ca}$  and  $\alpha$ -Mg matrix [12, 23].  $\text{Mg}_2\text{Ca}$  would be corroded preferentially at the beginning of the corrosion process. The seriously localized corrosion surround  $\alpha$ -Mn particles would also accelerate the spalling of  $\alpha$ -Mn and the formation of pitting holes (see in figure 8f). After the



addition of Sr, the microstructure of alloy was refined and the quantity of second phase is larger. Grain boundaries and second phases express less negative electrode potential compared with  $\alpha$ -Mg matrix because of the formation of Ca/Sr-rich phases [29], and the larger quantity of second phases did not cause more sites of micro-galvanic reaction. In the mean time, the compact grain boundaries and continuous distribution of  $\text{Mg}_{17}\text{Sr}_2$  along boundaries also block the corrosion of  $\alpha$ -Mg matrix because of the barriers effect. That means during the process of corrosion, hydrogen ions need to go around the grain boundaries to reach the corrosion interface and react with the active  $\alpha$ -Mg matrix, which increases the resistance of corrosion process. The similar phenomenon had also been reported in Mg-Al alloys [17, 33]. So, to Mg-1.5Mn-1Ca-1Sr alloy, the addition of Sr induced uniform anode consumption and decreased the corrosion rate.

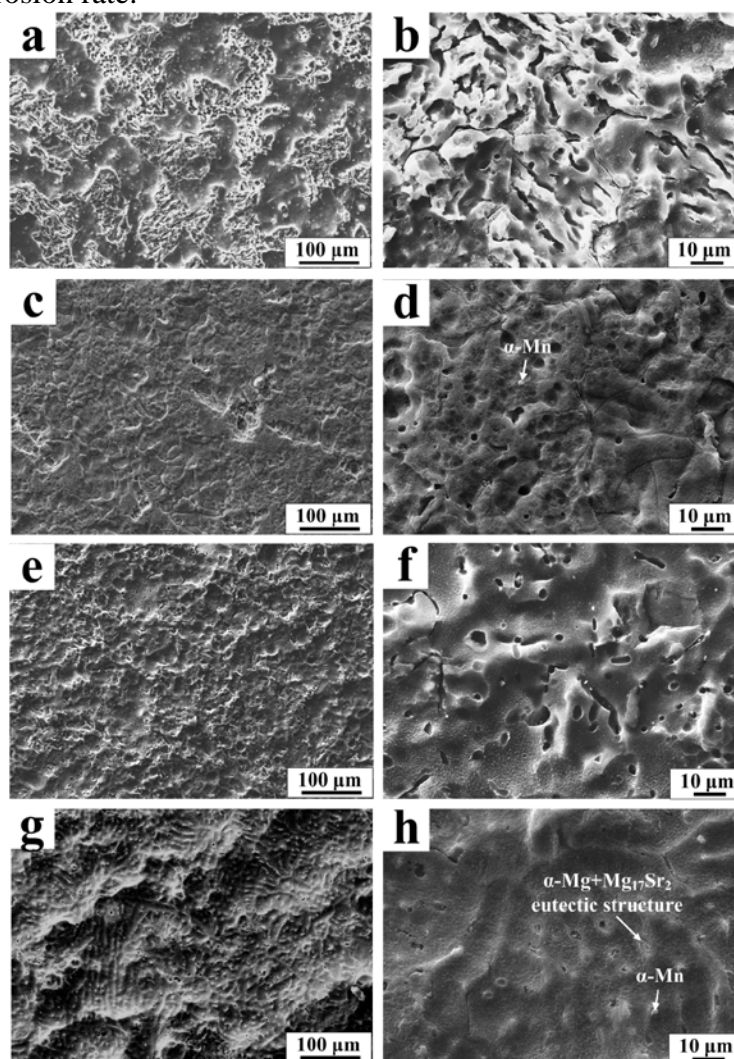


**Figure 8.** Surface morphology of Mg-1.5Mn-1Ca-xSr alloys immersed in SBF for 52 h after removed the corrosion products: (a & b) as-cast Mg-1.5Mn-1Ca alloy, (c & d) as-cast Mg-1.5Mn-1Ca-1Sr alloy, (e & f) T4 treated Mg-1.5Mn-1Ca alloy, (g & h) T4 treated Mg-1.5Mn-1Ca-1Sr alloy.

#### 4. Conclusions

Sr, Ca and Mn are naturally present in human body and the addition of these three alloying elements helped to reduce the grain size and formed  $\text{Mg}_2\text{Ca}$ ,  $\text{Mg}_{17}\text{Sr}_2$ , Ca/Sr-rich and  $\alpha$ -Mn phases in alloys, which reduced grain size and contributed to the increase of strength and corrosion resistance.

T4 treatment is a good way to improve both the mechanical properties and corrosion resistance of Mg-1.5Mn-1Ca-xSr alloys. By T4 treatment, solution strengthening effect and second phase strengthening effect simultaneously contribute to the improvement of tensile properties. The dissolution of  $\text{Mg}_2\text{Ca}$  in  $\alpha$ -Mg matrix not only decreases the fracture tendency but also reduces the sites of micro-galvanic reaction. The distribution of  $\alpha$ -Mn phase is more uniform and dispersive after T4 treatment, which help to resist severe localized attack.

By investigating on the corrosion behavior of Mg-1.5Mn-1Ca-xSr alloys, it could be summarized that corrosion first occurs in  $\text{Mg}_2\text{Ca}$  anode phase and  $\alpha$ -Mg matrix that surround the cathode phase. The corrosion behavior of Mg-1.5Mn-1Ca-xSr alloys is mainly controlled by the changes in quantity, distribution, configuration and size of the  $\text{Mg}_2\text{Ca}$ ,  $\text{Mg}_{17}\text{Sr}_2$  and  $\alpha$ -Mn phases. The  $\text{Mg}_{17}\text{Sr}_2$  and  $\alpha$ -Mn phases act as effective cathode induces micro-galvanic corrosion with  $\alpha$ -Mg matrix. The addition of Sr induced rather uniform anode consumption, which is mainly because the corrosion barrier effect caused by the compact boundaries and the uniformly distributed second phases. Finally, the suitable performances make T4 treated Mg-1.5Mn-1Ca-1Sr alloys possible to be potential biodegradable implant materials.

### Acknowledgements

This work is supported by the “985 Project” of Jilin University, the Science and Technology Program of Jilin Province (201105007), the Open Subject of State Key Laboratory of Rare Earth Resource Utilization (RERU2011001), the Science and Technology Support Project of Jilin Province (20130305008 GX) and the Science and Technology Support Project of Jilin Province (20140325003GX).

### References

- [1] Z Marciniak and K Kuczyński 1967 *International Journal of Mechanical Sciences* **9(9)** 609–620
- [2] R S Busk 1987 *Magnesium products design* M Dekker
- [3] B B Clow 1996 *Advanced materials & processes* Magnesium industry overview **150(4)** 33–34
- [4] M P Staiger, A M Pietak, J Huadmai and G Dias 2006 *Biomaterials* **27(9)** 1728–1734
- [5] N.-E Saris and E Carafoli 2005 *Biochemistry (Moscow)* **70(2)** 187–194
- [6] D Raftopoulos, E Katsamanis, F Saul, W Liu, and S Saddemi 1993 *Journal of biomedical engineering* **15(1)** 60–66
- [7] M Znamenskii 1945 *Khirurgiia* **12(1)** 60–63
- [8] G Song and A Atrens 2007 *Advanced Engineering Materials* **9(3)** 177–183
- [9] W H Organization 1996 Trace elements in human nutrition and health
- [10] W H Organization 1994 Assessing human health risks of chemicals: derivation of guidance values for health-based exposure limits/published under the joint sponsorship of the United Nations Environment Programme, the International Labour Organisation, and the World Health Organization
- [11] C K Yuen and W Y Ip 2010 *Acta biomaterialia* **6(5)** 1808–1812
- [12] N T Kirkland, N Birbilis, J Walker, T Woodfield, G J Dias and M P Staiger 2010 *Journal of biomedical materials research. Part B, Applied biomaterials* **95(1)** 91–100
- [13] H R B Rad, M H Idris, M R A Kadir and S Farahany 2012 *Materials & Design* **33** 88–97
- [14] F Rosalbino, S De Negri, A Saccone, E Angelini and S Delfino 2010 *Journal of materials science. Materials in medicine* **21(4)** 1091–1098
- [15] B Zhang, Y Hou, X Wang, Y Wang and L Geng 2011 *Materials Science and Engineering: C* **31(8)** 1667–1673
- [16] E Zhang and L Yang 2008 *Materials Science and Engineering: A* **497(1-2)** 111–118
- [17] L Wang, T Shinohara and B-P Zhang 2010 *Journal of Solid State Electrochemistry* **14(10)**

1897–1907

- [18] Y Jang, Z Tan, C Jurey, Z Xu, Z Dong, B Collins, Y Yun and J Sankar 2015 *Materials science & engineering. C, Materials for biological applications* **48** 28–40
- [19] M Salahshoor and Y Guo 2012 *Materials* **5(12)** 135–155
- [20] K Kannan, J Vetrano and C Hamilton 1996 *Metallurgical and Materials Transactions* **27(10)** 2947–2957
- [21] J A Helsen and H Jürgen Breme 1998 *Metals as biomaterials* (Wiley-VCH) pp
- [22] M Celikin, A A Kaya and M Pekguleryuz 2012 *Materials Science and Engineering: A* **550** 39–50
- [23] M Bornapour, N Muja, D Shum-Tim, M Cerruti and M Pekguleryuz 2013 *Acta biomaterialia* **9(2)** 5319–5330
- [24] S Dahl, P Allain, P Marie, Y Maturas, G Boivin, P Ammann, Y Tsouderos, P Delmas and C Christiansen 2001 *Bone* **28(4)** 446–453
- [25] P Marie 2005 *Osteoporosis international* **16(1)** S7–S10
- [26] A Taylor 1985 *Clinics in endocrinology and metabolism* **14(3)** 703–724
- [27] G Song and A Atrens 2003 *Advanced engineering materials* **5(12)** 837–858
- [28] Y Lee, A Dahle and D StJohn 2000 *Metallurgical and Materials Transactions A* **31(11)** 2895–2906
- [29] M Bornapour, M Celikin, M Cerruti and M Pekguleryuz 2014 *Materials science & engineering. C, Materials for biological applications* **35** 267–282
- [30] B Brindley and P Worthington 1970 *International Materials Reviews* **15(1)** 101–114
- [31] Y Chino, M Kobata, H Iwasaki and M Mabuchi 2002 *Materials Transactions* **43(10)** 2643–2646
- [32] G Yu, Y-L Liu, Y Li, L-Y Ye, X-H Guo and L Zhao 2002 *Chinese Journal of Nonferrous Metals* **12(6)** 1087–1098
- [33] Y J Ko, D Y Chang, J D Lim and K S Shin 2003 *Materials Science Forum* 851–856